Available on CMS information server

CMS NOTE 1999/056

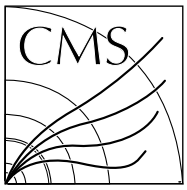

The Compact Muon Solenoid Experiment

CMS Note

Mailing address: CMS CERN, CH-1211 GENEVA 23, Switzerland

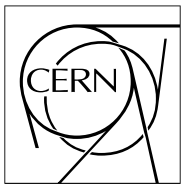

22 October 1999

Study of $\mathrm{dE/dx}$ Measurements with the CMS Tracker

S. Banerjee[a)], A. Caner[b)], S. Dutta[c)], A. Khanov[b,d)], F. Palla[c)], G. Tonelli[c)]

Abstract

We report in this note a study of particle identification by pulse height information in the CMS tracker, in the context of isolated tracks as well as tracks inside a hadron jet. We have used the simulation package CMSIM and the tracker layout described in the Technical Design Report. We describe the discrimination efficiency between π and K as well as the electron identification capability of the stand-alone CMS tracker.

[a)] Tata Institute of Fundamental Research - EHEP, Mumbai

[b)] CERN, European Laboratory for Particle Physics, Geneva

[c)] University of Pisa and INFN, Pisa

[d)] On leave from ITEP, Moscow, Russia

1 Introduction

The measurement of energy loss through ionisation can be an important tool in many physics analyses. Particle identification can also improve track reconstruction, as in the case of electrons for which the effects of bremsstrahlung have to be taken care of. In this note, we try to investigate the possibility of $\mathrm{dE/dx}$ measurement in the proposed tracker of the CMS experiment [1]. The note is organised as follows. Section 2 describes some details of simulation of the CMS tracking detector. Reconstruction of tracks and method of determination of $\mathrm{dE/dx}$ are given in sections 3 and 4. The measurement of $\mathrm{dE/dx}$ for single tracks is discussed in section 5 and its implementation for electron identification in realistic physics environment is presented in section 6. Section 7 summarises the results of this study.

2 Detector Simulation

2.1 Detector layout

Simulation of the CMS tracker has been carried out by the CMSIM [2] program, version 114, using the general purpose detector simulation tool GEANT3 [3]. The detector description in CMSIM closely follows the Technical Design Report of the various major subsystems of the tracker [4].

The CMS tracker consists of three major subsystems: a silicon pixel detector close to the interaction point, a silicon strip detector in the intermediate region and a tracker system based on micro-strip gas chambers (MSGC's) extending to an outer radius of 116 cm. Figure 1 shows the layout of the detector planes. Each sub-detector has a central component where the detectors are arranged on coaxial cylinders and the forward-backward part where detector stations are arranged in disk-like layers. In the picture, darker segments represent double-sided detectors providing 3-dimensional points, whereas lighter marks show sensors providing cluster coordinates in the bending plane.

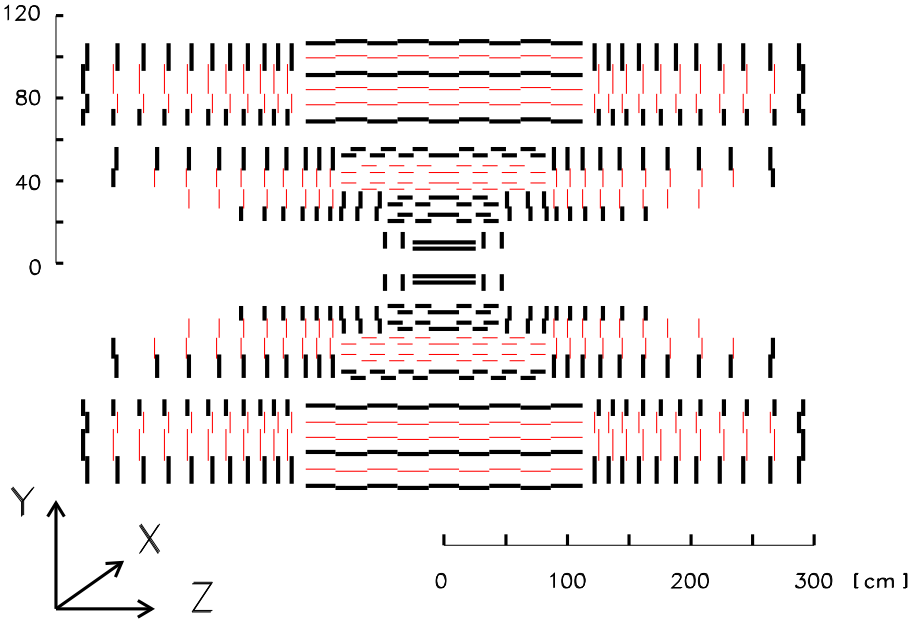

Figure 1: Layout of the detector planes of the CMS tracker as in the CMSIM 114 geometry

The two layers (disks) of pixel detectors are equipped with 250 μm thick silicon wafers with pixel size 125 μm $\times$ 125μm. Silicon strip detectors are used to instrument 5 cylindrical layers and 10 disks of end-cap detectors on either side. The two innermost layers of silicon barrel detectors are complemented by 3 stations of mini end-caps on either side. The third and fourth layers of the barrel detectors and the two middle rings of the forward-backward detectors are single sided detector elements while the rest are double sided ones. The entire system is based on 300 μm thick, single-sided silicon wafers; space points are measured by pairs of single-sided detectors mounted back to back. The MSGC system includes six equidistant layers in the barrel and eleven stations with 4-fold segmentation in both end-cap regions. Three layers and two forward rings (see figure) are equipped with single sided chambers while the remaining stations are instrumented with twin chambers mounted back to back for stereo

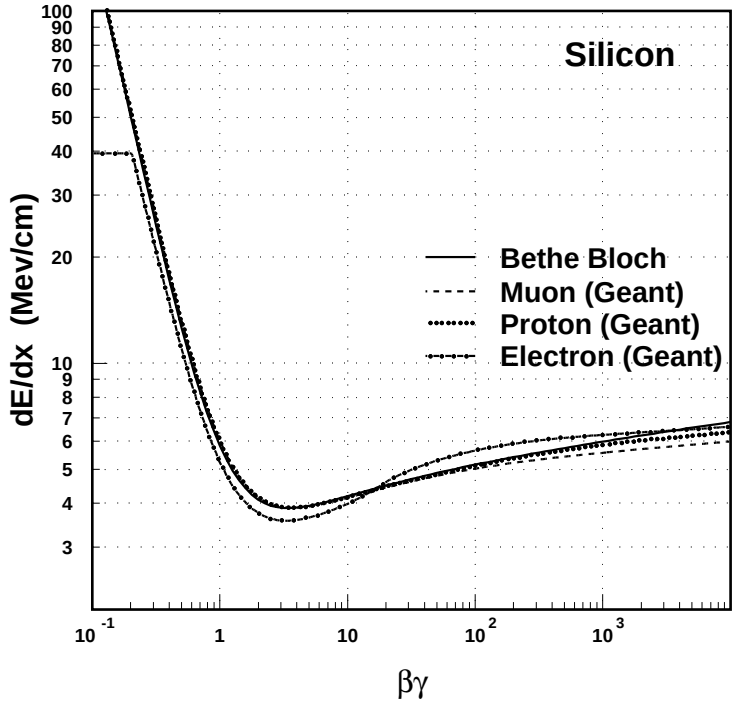

Figure 2: Differential energy loss by ionisation as a function of $\beta\gamma$ in silicon. The solid line is as expected from Bethe-Bloch formula and the dashed, dotted and dashed-dotted lines are from energy loss table as in GEANT3 for muons, protons and electrons with the cuts as described in the text

measurements.

2.2 Detector response

The energy lost by charged particles while traversing the sensitive part of the detector element is collected and digitised according to the prescriptions documented in [4], Chapter 7, Sections 8, 9, 10. The continuous energy loss in the sensitive part of the detector has been simulated without generation of δ-rays and with full Landau-Vavilov fluctuation. This procedure gives a better description of the energy loss in thin materials. The cutoff in kinetic energy has been set to 10 KeV for electrons and photons in the sensitive material. The dependence of the energy loss on the particle momentum is given by the Bethe-Bloch formula [5]. The $\mathrm{dE/dx}$ in silicon is plotted in Figure 2 as a function of $\beta\gamma$ of the particle. In the same plot, we also shows energy loss per unit length as has been used in the simulation for muons, protons and electrons. The energy loss for heavy particles agree with Bethe-Bloch up to $\beta\gamma$ values of 100, the ranges probed in this report. The dependence due to particle mass is due to including the photon energies below kinematic cutoff for bremsstrahlung process [6] set to 10 MeV in our studies.

Electronic noise is generated as Gaussian fluctuations of null pedestal values. There is no attempt to handle pedestal subtraction. Further, the "common mode" fluctuations observed in beam tests are also not reproduced by the simulation package. The signal to noise values used in this study are $\approx$ 10, 20 for silicon strip and MSGC detectors respectively. [1)] The Pixel noise is $\approx 270\ e^-$ per channel to be compared to a cluster charge of typically 20000 e^- (mip at normal incidence). The digitisation is made by 11-bit ADC's for silicon strip and MSGC detectors, 8-bit ADC for the the Pixels (9-bit for the end-caps). The dynamical range is about 10.5 mips for silicon strips, 1.6 for MSGC and pixel detectors. In CMS, we expect to use 8-bit ADC's to map a dynamical range not fully defined as of yet. It is nevertheless clear that a correct simulation of the digitisation is mandatory to estimate the $\mathrm{dE/dx}$ resolution and will be implemented as the ADC specifications are better understood.

[1)] The S/N ratio is defined here by the ratio of the total reconstructed cluster charge to the average noise of a single strip.

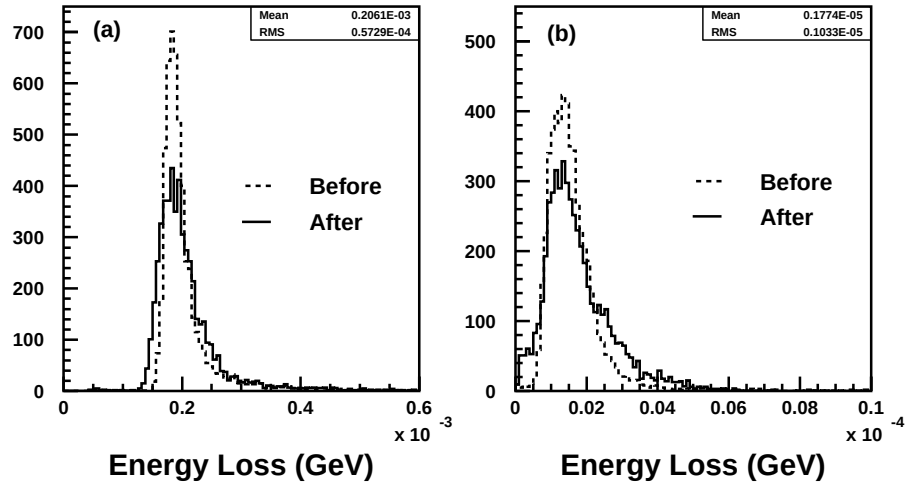

Figure 3: Energy loss distribution for a 3 GeV electron at pseudo-rapidity η = 0.8 in (a) silicon and (b) MSGC detectors before digitisation and after cluster reconstruction.

3 Reconstruction

In the following we will refer to 'hit' or 'cluster' to indicate fully digitised signals filtered by the reconstruction algorithms. By 'impacts' we will indicate the simulated hits prior to digitisation.

Suitable clustering algorithms, as described in [4], with thresholds for seed and shoulder strips as well as for the total cluster charge, are used to define the released energy and to reconstruct the hit position. The performance of the clustering algorithms have been validated with test beam data. Whenever possible, 3-dimensional cluster coordinates are measured by matching the information from (r, ϕ) and stereo detectors. Tracks are reconstructed using the GTF (Global Track Finder) algorithm [4], Chapter 8. Starting with preselected roads, a backward propagating Kalman filter is used to carry out the final selection of hits and fit the track trajectory through the associated clusters. Typically a track finding efficiency larger than 95% for isolated tracks and above 90% for tracks in jets is estimated, when the track transverse momentum satisfies $\mathrm{p_T} > 1$ GeV. In this analysis, a reconstructed track is required to have at least 8 hits registered in the detector. Moreover, we require for this study that at least 5 hits be generated in silicon detectors. Pairs of hits in back-to-back sensors that have been associated by the pattern recognition, i.e. 3D clusters, are counted as 2 hits.

The converted charge after digitisation is used for the determination of $\mathrm{dE/dx}$. The energy loss of a track can be constructed from the hits as well as from the impacts associated to the track by the fitting procedure. The digitised pulse height and the estimated path length across the detector, calculated taking into account the track orientation, allow to estimate the energy loss and $\mathrm{dE/dx}$ with the information available after reconstruction. Each hit can be associated to its parent impact so that the true deposited energy and stub length across the sensor can be retrieved from the Monte Carlo and used to provide the true energy loss and $\mathrm{dE/dx}$. The reconstructed and simulated energy loss of 3 GeV electrons in silicon and MSGC detectors are shown in Figure 3. The smearing effect of digitisation and cluster reconstruction are visible.

To estimate the absolute calibration constants K, [K]= KeV/ADC count, for the three subsystems, we have compared the pulse heights of the hits measured in ADC counts to the impact energy, as shown in Figure 4. Comparing the means of two such distributions for each of the sub-detectors, we obtain calibration values K = 0.5 KeV/ADC count for silicon sensors and K $\approx$ 1 eV/ADC count for MSGC's.[2)]

No attempt is made in this study to address a realistic calibration study. The tolerances of the silicon wafers, the channel-to-channel gain variation, imperfect control of noise and common mode, non-full depletion, as well as the very large number of readout channels will render the energy calibration of the tracker a challenging task. All these effects can be simulated and will be addressed in further analyses. Within the present modelling limitations, the simulated and reconstructed energy loss distribution for silicon detectors are indeed very similar. For the MSGC system, the similarity holds but for low $\mathrm{p_T}$ tracks. For these tracks, the angle of incidence on the detectors become

[2)] The MSGC calibration has been obtained comparing the cluster pulse height in ADC counts to the energy deposition in KeV as calculated by GEANT3 rather than to the estimate of the stand-alone simulation of the MSGC response.

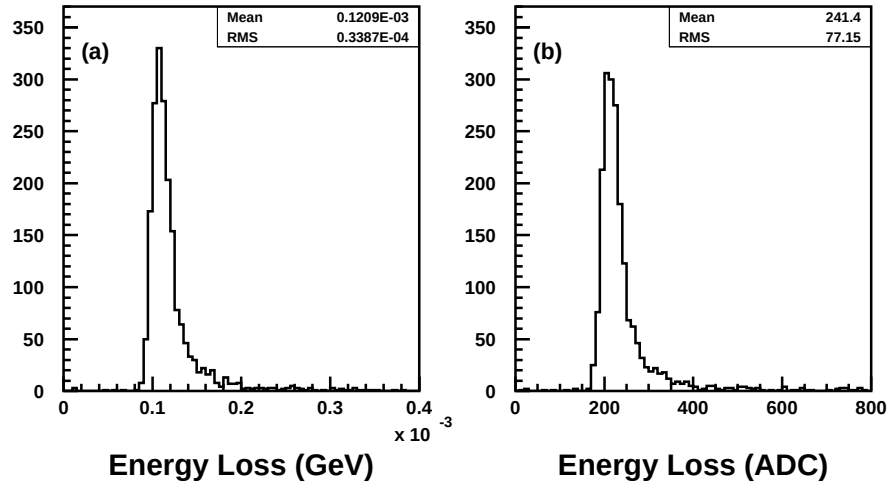

Figure 4: Raw energy loss distributions from (a) simulated impacts (in GeV) and (b) reconstructed hits for a 3 GeV muon in the pixel detector

large, especially at the largest radii of the tracker. The modest ionisation multiplicity and its large statistical fluctuations affect the capability to fully reconstruct large size clusters, which may split or have most of the strips below threshold. Typically, tracks with $\mathrm{p_T}$ of 1 GeV generate clusters of true size 12 ± 3.8 strips in the outer barrel layer, which reduces to 2.7 ± 1.9 after cluster reconstruction. The recovery of these cluster for a better energy measurement appears to be non trivial. The clustering algorithm requires each adjacent strip to collect charge in excess of 1.8 times the noise (σ) and a seed strip with pulse height larger than 3 times the strip noise. If one lowers the shoulder threshold to 1.4 σ, the reconstructed cluster size increases to 6.3 ± 3.0. These clusters, are affected, on average, by a missing strip in 62 % of the cases, where a missing strip is defined as a strip which has collected charge below shoulder threshold. In a quarter of these cases, the missing strip is adjacent to the seed strip and contributes to underestimate the cluster energy by 32 %. In the remaining cases, the energy is underestimated by 22 %. Allowing for one missing strip in hit reconstruction leads to add to the clusters a spurious strip (noise) 11 % of the times. This spoils the cluster energy measurement and adds on average 17 % of the energy value contributed by noise. Figure 5 compares the distributions of reconstructed and simulated $\mathrm{dE/dx}$ measurements in MSGC for 1 GeV electrons. When allowing for one missing strip, the energy measurement is somewhat improved, but the resolution appears to be very poor. However, this effect decreases with energy and becomes negligible when $\mathrm{p_T}$ is larger than $2 \div 3$ GeV.

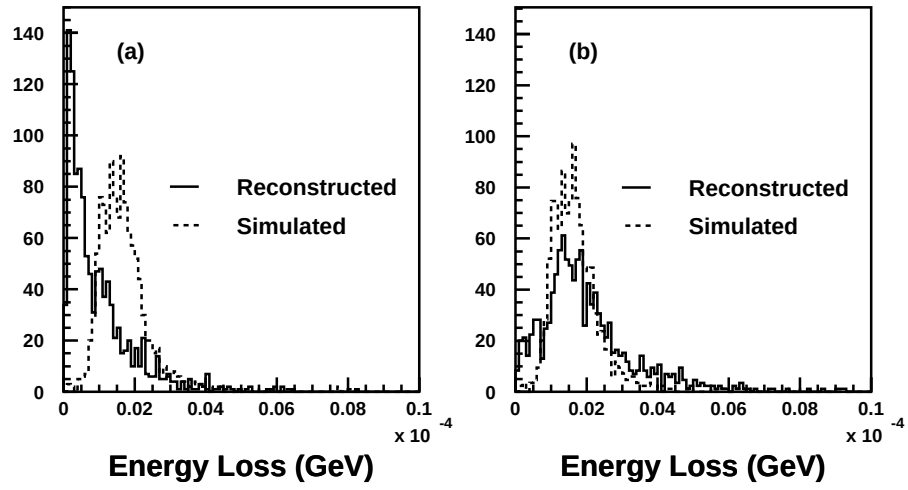

Figure 5: Energy loss distributions from simulated and reconstructed hits for a 1 GeV electron in MSGC with (a) no missing strips allowed (b) one missing strip allowed in the cluster

4 Determination of $\mathrm{dE/dx}$

The $\mathrm{dE/dx}$ distribution is always characterised by a long tail as can be seen in Figure 6(a) for a 5 GeV muon in the silicon strip detector. The large tail will automatically induce a large uncertainty in the mean of the distribution. We have tried two methods to improve the resolution of the mean $\mathrm{dE/dx}$ measurement:

1. In the first method, we use the tail truncation approach by rejecting a given fraction of the highest energy measurements. The fraction has been varied from 20% to 40% and the corresponding changes in resolution are summarised in Table 1.

2. In the second method, we first compute the mean and the RMS using all the samplings of a given track and then compare each of them with its mean value. We retain a measurement if it is smaller than (Mean $+$ 1.5 $\times$ RMS). The mean $\mathrm{dE/dx}$ is then recomputed using the retained set of measurements.

Figures 6(b) and (c) show the $\mathrm{dE/dx}$ distributions obtained applying the above two methods for a 5 GeV muon. Tail truncation yields a substantial improvement in $\mathrm{dE/dx}$ resolution. With the second method, we obtain the best RMS and a determination of the most probable value that is closer to the one of the unbiased distribution. Nevertheless, in the present study we just adopt the traditional approach, i.e. the first method with 40% rejection, which makes no assumption on the parent population statistics. Further refinements will be studied in future work, also concerning the low energy tail of the $\mathrm{dE/dx}$ distribution that has lower purity due to noise contributions.

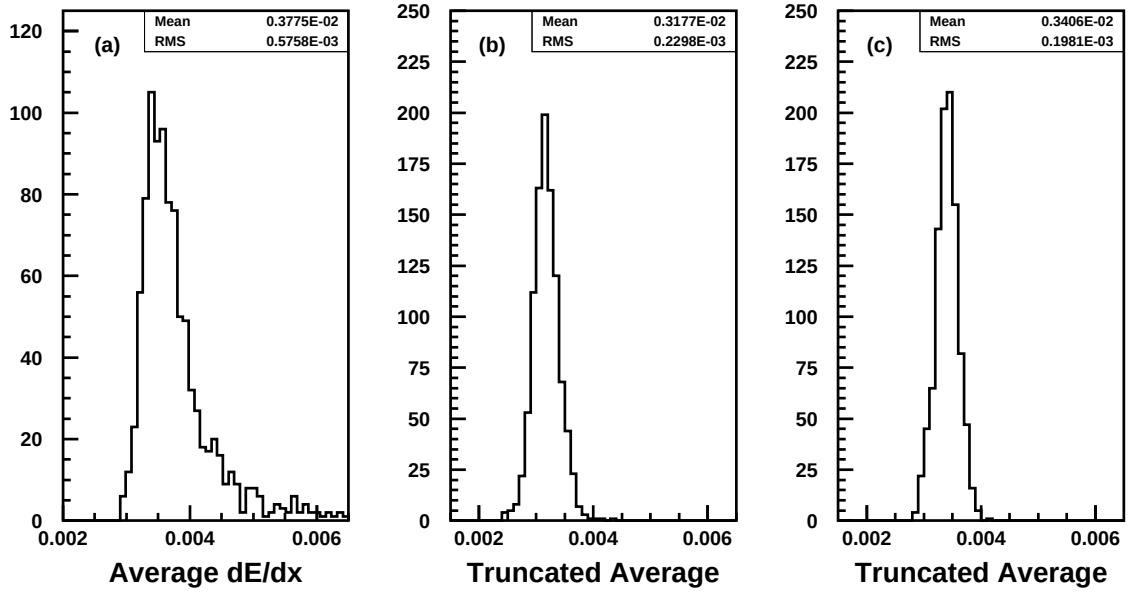

Figure 6: Average $\mathrm{dE/dx}$ measurement in GeV/cm for a 5 GeV muon in the silicon strip detector (a) without rejecting any measurements, (b) rejecting 30% of the measurements on the higher side, (c) rejecting measurements larger than (Mean + 1.5$\times$RMS)

The $\mathrm{dE/dx}$ measurements from the two types of silicon detectors (pixels and strips) can be directly combined and treated as a single data sample since they have a common mean and similar resolutions. All hits in silicon sensors are then grouped, tail truncation is applied and the mean $\mathrm{dE/dx}$ is retrieved. Incidentally, the distributions are pseudo-Gaussian and there is no appreciable difference in considering the most probable rather than the mean value. The $\mathrm{dE/dx}$ measurement with MSGC's has a much poorer resolution ($\approx$ 20%) and a 3 orders of magnitude smaller energy scale. One can develop appropriate likelihoods to combine measurements in gas and silicon sensors, still the most precise estimate when combining data with different errors is given by their weighted mean. By using a suitable calibration factor to scale the $\mathrm{dE/dx}$ in MSGC to that in silicon one can estimate:

$$M = \frac{\sum_i W_i \cdot M_i}{\sum_i W_i}$$

$$\sigma = \sqrt{\frac{1}{\sum_i W_i}}$$

Source	Method	Mean (GeV/cm)	RMS (GeV/cm)	Resolution (%)
3 GeV μ^+	All measurements	0.377×10^{-2}	0.542×10^{-3}	14.38
	Truncation (20%)	0.320×10^{-2}	0.233×10^{-3}	7.28
	Truncation (30%)	0.311×10^{-2}	0.203×10^{-3}	6.53
	Truncation (40%)	0.302×10^{-2}	0.186×10^{-3}	6.16
	Method (2) of text	0.327×10^{-2}	0.172×10^{-3}	5.26
10 GeV μ^+	All measurements	0.397×10^{-2}	0.537×10^{-3}	13.53
	Truncation (20%)	0.349×10^{-2}	0.233×10^{-3}	6.68
	Truncation (30%)	0.340×10^{-2}	0.204×10^{-3}	6.00
	Truncation (40%)	0.331×10^{-2}	0.193×10^{-3}	5.83
	Method (2) of text	0.355×10^{-2}	0.176×10^{-3}	4.96

Table 1: Comparison of resolution in $\mathrm{dE/dx}$ for muons in the silicon strip detector using different methods

where M_i are the mean values from the two separate measurements (scaled up in the case of MSGC's) and the weight factor W_i is related to the corresponding RMS values σ_i through:

$$W_i \quad = \quad \frac{1}{\sigma_i^2}$$

Considering a typical $\mathrm{dE/dx}$ resolution of 6% and 20% for silicon and MSGC detector groups and the above error expression one obtains a resolution on the combined measurement of 5.8%. The MSGC detector does not appear to improve the $\mathrm{dE/dx}$ resolution as will be confirmed in the following sections. It is though reasonable to consider that the extra number of hits measured by the MSGC detector contribute some robustness to the $\mathrm{dE/dx}$ measurement in case of silicon hit inefficiency and further that long-lived particles are predominantly sampled by the MSGC tracker (e.g. K^0_s, conversions).

5 Single Tracks

To analyse the performance of the $\mathrm{dE/dx}$ measurement in the CMS tracker, we have generated single particles with different momenta at a fixed pseudo-rapidity η = 0.8. The primary vertex position has been smeared according to Gaussian statistics, modelling a beam spot size of 15 μm in the transverse plane and 5.3 cm along the beam direction. Six different momentum values have been used: 1, 2, 3, 4, 5 and 10 GeV. Five particle types (e^+, μ^+, π^+, K^+ and p) have been studied.

Table 2 summarises the effect of combining measurements from the different tracker subsystems on the resolution of $\mathrm{dE/dx}$ for isolated μ^+ tracks. One sees that there is a significant gain in combining the measurements from pixel and silicon strip detectors. MSGC's, which measures $\mathrm{dE/dx}$ with a much poorer resolution, do not contribute significantly to the overall measurement of $\mathrm{dE/dx}$. For particle of low momentum ($\mathrm{p_T} < 2 \div 3$ GeV) the resolution is affected by cluster splitting.

Momentum (GeV)	Resolution in (%)				
	Pixel	Silicon	Silicon+Pixel	MSGC	All Tracker
1.0	11.82	8.21	6.94	68.67	
2.0	11.08	8.03	6.64	35.08	
3.0	11.74	7.46	6.15	26.82	6.01
4.0	11.61	7.79	6.37	22.99	6.15
5.0	10.06	7.23	6.04	20.94	5.81
10.0	10.89	7.37	5.83	20.03	5.60

Table 2: Resolution in $\mathrm{dE/dx}$ measurements for isolated μ^+ using subsystems of the CMS tracker

Table 3 summarises the resolutions in $\mathrm{dE/dx}$ measurements for different particle types as a function of track momentum. The resolution does not depend strongly on the particle type or on particle energies. However, there is a weak improvement of the resolution at larger energies.

Figure 7 shows the average $\mathrm{dE/dx}$ estimated by using the pixel and silicon strip detectors as a function of particle momentum for the five different particle types. In Figure 7(a) we show the measurements from reconstructed

Momentum (GeV)	Resolution in (%)			
	e^+	π^+	K^+	p
1.0	7.44	7.03	8.32	8.76
2.0	6.53	6.83	7.06	8.89
3.0	6.44	6.71	6.74	7.32
4.0	6.33	6.15	7.03	7.09
5.0	6.27	6.12	6.61	6.98
10.0	6.38	5.96	6.34	6.82

Table 3: Resolution in $\mathrm{dE/dx}$ measurements for isolated particles using the pixel and silicon strip detectors of CMS

hits, which are compared to the estimates obtained from impacts for electrons and pions in Figure 7(b). The measurements from reconstructed hits are within 10% from the ideal measurements. The difference gets smaller at higher momenta. It seems to be mainly due to lack of tail truncation at the lower side of the energy loss distribution. The true energy loss shows a Landau distribution with a tail only on the higher side, whereas that from reconstructed hits shows a tail also on the lower side of the spectrum, decreasing with incident energy. This behaviour needs to be better understood. In fact, at low momentum hits generated in silicon detectors have rather large cluster size due to the angle of incidence on the sensors. Some of the strips may collect an amount of charge which fluctuates below the threshold. In the studied momentum range, one can see the tail of $1/\beta^2$ fall in $\mathrm{dE/dx}$ for protons and kaons, but for all other particles only the relativistic rise part is sampled.

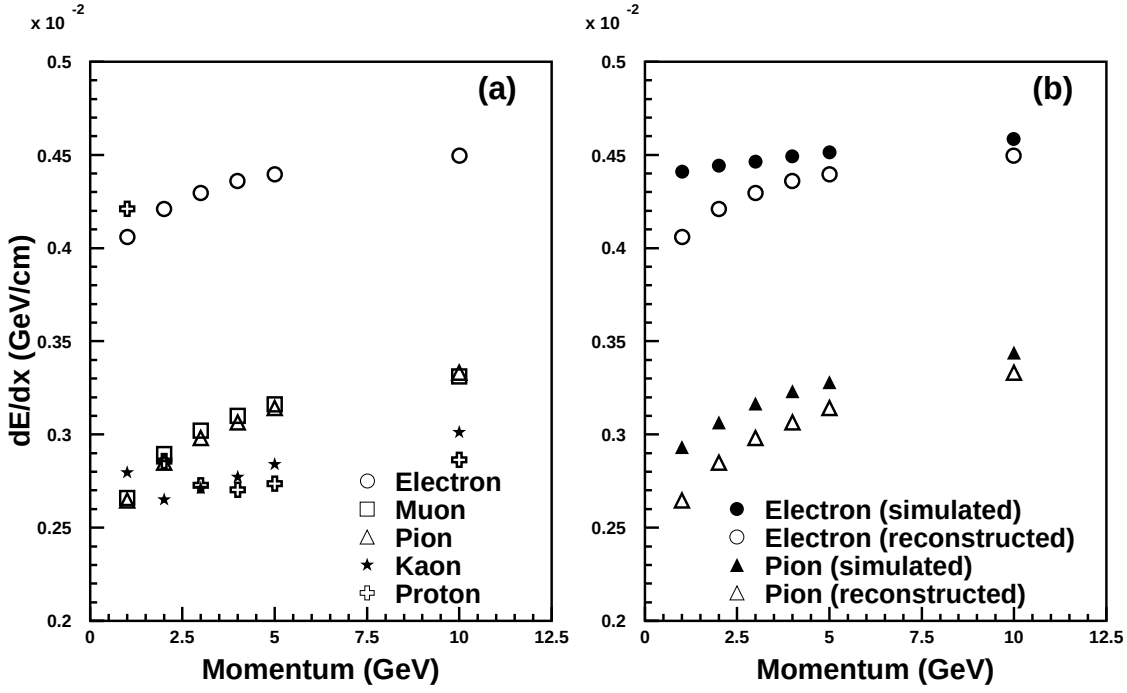

Figure 7: (a) Mean $\mathrm{dE/dx}$ as a function of particle momentum for different particle types as measured from reconstructed hits. (b) Comparison of mean $\mathrm{dE/dx}$ as measured from reconstructed and simulated hits for electrons and pions as a function of momentum.

The discriminating power for any two given particle types can be measured by the ratio of the difference in the mean $\mathrm{dE/dx}$ for the two particles to the mean spread in $\mathrm{dE/dx}$ measurement. We define this ratio to estimate the significance of discrimination (D).

$$D = \frac{|\,\mathrm{dE/dx_1} - \mathrm{dE/dx_2}\,|}{\mathrm{RMS}}$$

We have chosen the RMS in $\mathrm{dE/dx}$ distribution obtained for pions at the corresponding momentum as the mean spread. Figure 8 shows the significance in discriminating power as a function of particle momentum for (a) the π/K and (b) the e/μ hypotheses. The discrimination between the e/μ hypotheses is rather large (> 5), whereas

the separation between π and K hypothesis is marginal ($\approx$ 1.5). Additional use of MSGC measurements slightly improves the situation (to a value of $\approx$ 1.8). The $\mathrm{dE/dx}$ cross-over for π and K appears to be at a momentum of $\approx$ 1 GeV.

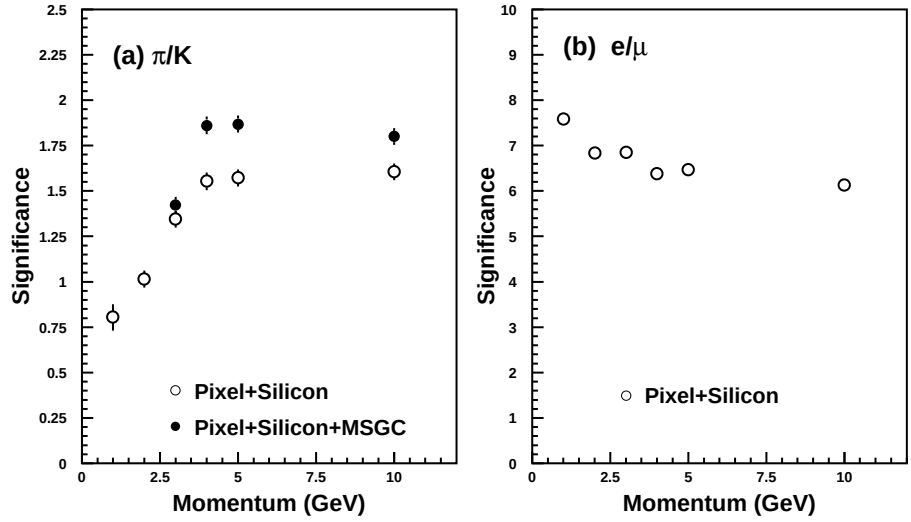

Figure 8: Discrimination between particle types as a function of particle momentum for (a) π/K and (b) e/μ hypotheses. Also shown for π/K hypotheses, the discrimination factors if MSGC measurements are used in addition. The $\mathrm{dE/dx}$ cross-over for π and K is around 1 GeV as shown by the fit.

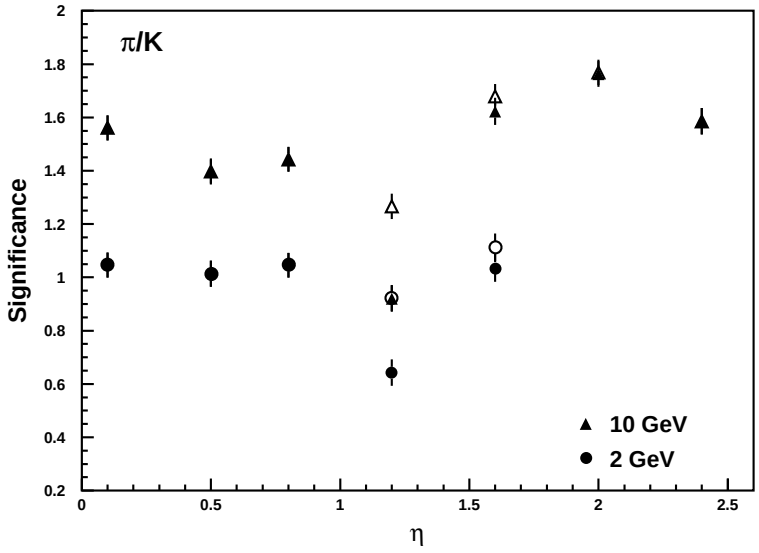

Figure 9: Discrimination between π/K mass hypotheses as a function of pseudo-rapidity for two different momenta. The closed (open) points are obtained without (with) applying the additional fudge factor as explained in the text.

We looked into discrimination of particle types as a function of the angle of incidence of the track. Particles have been generated at several η values (0.1, 0.5, 0.8, 1.2, 1.6, 2.0 and 2.4) and the resulting discrimination for π/K hypothesis as a function of η is shown in Figure 9 for two different particle momenta. The discrimination stays constant in the barrel part of the detector, deteriorates in the transition region and subsequently improves in the forward region. The rise at large η can be explained with the number of samplings in silicon which increases from η = 1.4 up to η = 2.2 (Figures 10, 11). We have examined the deterioration around η = 1.2 in great detail. This region has a mixture of 3 detector types, barrel, mini-endcap, endcap detectors and also the tracks see the cables from inner detectors at least twice. Interactions in this additional material deteriorates the resolution by $\approx$ 6%. On the other hand, a track traverses different lengths in silicon, ranging from 350 to 550 μm in this region, and one sees the mean $\mathrm{dE/dx}$ to have a step at around 480 μm. This behaviour is observed in the true $\mathrm{dE/dx}$ and is

probably introduced due to lack of matching of the different algorithms used in GEANT3 for description of energy loss in thin materials. This problem is under investigation [6]. On the other side, if we compensate this shift in the mean by a fudge factor, the drop in discrimination at η around 1.2 is largely balanced as can be seen in the Figure 9.

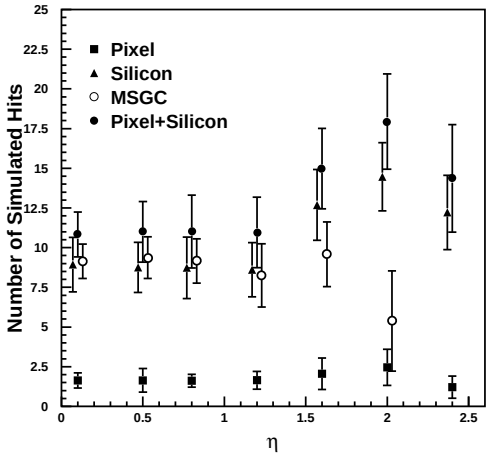

Figure 10: Impacts per track crossing the detector as a function of η.

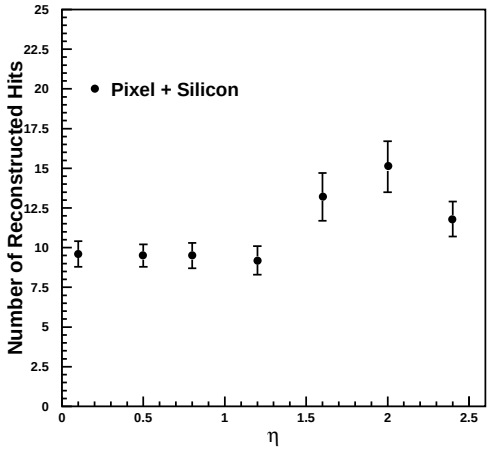

Figure 11: Reconstructed hits associated to fitted tracks as a function η in the Silicon Tracker.

6 Electron Identification

Based on the above studies we use the discrimination parameter as a tool for particle identification. Since the discrimination of π from K is not very good, we restrict ourselves to the identification of electrons. The CMS electro-magnetic calorimeter is a powerful tool for electron identification, but it has high efficiency only for high energy electrons, while the combined performance of ECAL and Tracker could be used to identify electrons over the full range of reconstructed momenta. Lower energy electrons could be of interest for example in B-physics where one of the B-hadrons decays semileptonically to an electron.

For a track of given momentum, the reconstructed $\mathrm{dE/dx}$ value (truncated mean after rejecting 40% of the measurements) is compared with the corresponding value for electrons of similar energy. This requires interpolation from a table of such measurements, derived from single electron track simulation in the present study, possibly from data at running time. If the difference (interpolated $-$ measured) is smaller than 2 times the RMS in $\mathrm{dE/dx}$ for electrons (again using an interpolation table), the track is identified as an electron. The remaining tracks are classified as hadrons or muons.

The above electron identification criterion has been applied to two different types of event samples. The first sample consists of B_s pairs produced using the PYTHIA event generator. We require that one of the B_s decays semileptonically to electron and the other decays as $J/\psi\phi \rightarrow \mu^+\mu^- K\bar{K}$. We demand there should be at least 2 muons with $\mathrm{p_T} > 4$ (2) GeV in the barrel (forward) detector and the transverse momenta of hadrons and electrons to be larger than 1 GeV. This reaction produces a sample of soft electrons. The overall and transverse momentum spectra of the electron sample is shown in Figure 12.

Reconstructed tracks are associated to the generated parent tracks by shared hits. The particle type which is responsible for the maximum number of hits contributing to the reconstructed track is used for identification. For momentum larger than 1.5 GeV, we find the selection efficiency of electrons to be $97.7 \pm 0.5\%$ and the rejection efficiency of non-electrons to be $99.85 \pm 0.03\%$. A detailed break-down of the different particle types and number of 'electron' candidates in each category from a sample of 1200 events is summarised in Table 4.

It is interesting to gauge the identification capability also in high track density environments, when a larger probability of wrong hit assignment or hit merging degrades the $\mathrm{dE/dx}$ measurement. To study electron identification within high $\mathrm{E_T}$ jets, several samples of $b\bar{b}$ events with $\mathrm{E_T}$ ranging from 50 GeV to 200 GeV were generated in

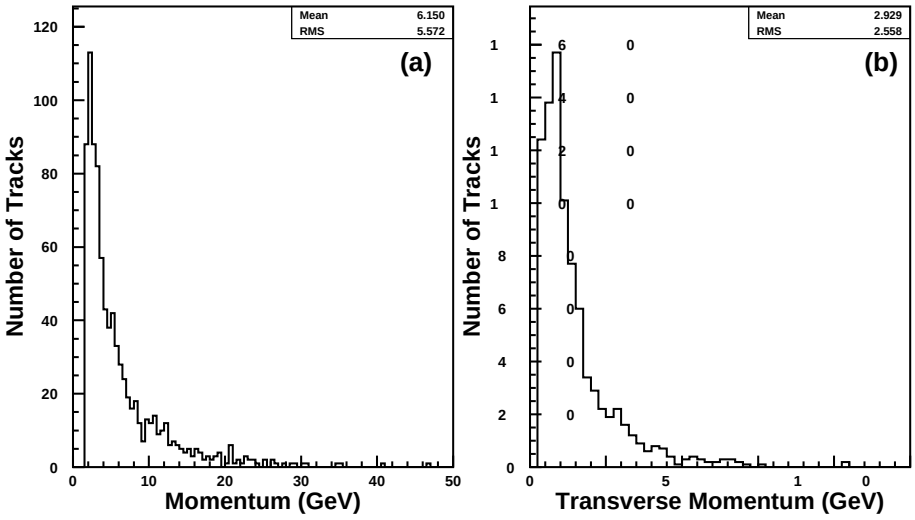

Figure 12: (a) Momentum and (b) transverse momentum spectrum of electrons from the B_s sample where the electrons come from semileptonic decays of B_s

	e	μ	π	K	p
Preselected Tracks by ID	842	2027	7986	2258	1171
'Electron' Candidates	823	7	18	1	22
Discrimination Efficiency (%)	97.7	99.6	99.8	99.9	98.1

Table 4: 'Electron' discrimination efficiency for different particle types in the B_s event sample

the pseudo-rapidity interval $|\eta| < 2.5$. Here we present results for three different $\mathrm{E_T}$ values (50, 100 and 200 GeV) corresponding to event samples of 2500, 2500 and 1923 events. We obtain electron selection efficiencies of 95.6 ± 0.4%, 93.3 ± 0.4% and 90.6 ± 0.4% at the three different jet $\mathrm{E_T}$'s. The corresponding rejection rates are 99.79 $\pm$ 0.02%, 99.56 $\pm$ 0.03% and 98.67 $\pm$ 0.04%, respectively. The break-down of 'electron' identification performance according to particle type is summarised in Table 5 for the different $\mathrm{E_T}$ values. In the first row we show the number of reconstructed tracks with at least 6 hits in silicon sensors (i.e. preselected) by particle type. Electron candidates satisfy the $\mathrm{dE/dx}$ identification requirements. Efficiency for finding such electron tracks (as defined in [4]) does not depend critically on the jet $\mathrm{E_T}$, having a value around 75%. This number clearly depends on the event topology and is somewhat less for soft electrons as from B_s decays. The track finding efficiency ranges between 65% and 75% in all topologies of interest.

Jet $\mathrm{E_T}$		e	μ	π	K	p
50 GeV	Preselected Tracks by ID	2651	1086	38357	7532	3775
	'Electron' Candidates	2533	3	116	5	40
	Discrimination Efficiency (%)	95.5	99.7	99.7	99.9	98.9
100 GeV	Preselected Tracks by ID	4660	1040	51300	9319	4721
	'Electron' Candidates	4349	5	303	15	52
	Discrimination Efficiency (%)	93.3	99.5	99.4	99.8	98.9
200 GeV	Preselected Tracks by ID	6220	735	51443	8500	4667
	'Electron' Candidates	5635	6	745	77	61
	Discrimination Efficiency (%)	90.6	99.2	98.6	99.1	98.7

Table 5: 'Electron' discrimination efficiency for different particle types in the $b\bar{b}$ jet samples at 3 different $\mathrm{E_T}$ values. In the first raw we list the number of reconstructed tracks with at least 6 hits in silicon sensors (i.e. preselected) by particle type. Electron candidates satisfy the $\mathrm{dE/dx}$ identification requirements.

Figure 13 shows electron selection efficiency and rate of contamination of non-electron particles as a function of the particle $\mathrm{p_T}$. The selection efficiency is rather independent of particle momentum, but the purity of track identification in high $\mathrm{E_T}$ jets tends to degrade with track $\mathrm{p_T}$.

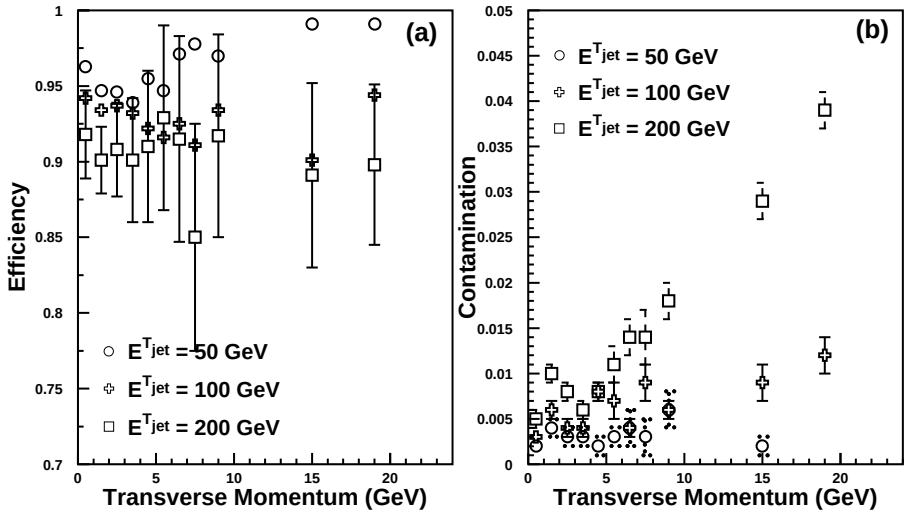

Figure 13: (a) Selection efficiency of electrons and (b) contamination of non-electron tracks identified as electrons as a function of track $\mathrm{p_T}$ for three different jet $\mathrm{E_T}$ values

The electron selection efficiency as well as the efficiency to reject non-electron tracks deteriorates for larger $\mathrm{E_T}$ jets. Within these jets the probability of wrong hit assignment is non-negligible. We show in Figure 14(a) the fraction of hits of the reconstructed track correctly associated to the generated parent electron as a function of track transverse momentum, for different jet $\mathrm{E_T}$'s. To define a hit as correctly associated we require that the corresponding impact is generated by the electron parent track. Reconstructed hits for which other impacts contribute to the pulse height together with the electron impact (i.e. merged hits) are also considered as good hits. In this study we do not distinguish when electron hits overlap to other primary tracks or to secondaries (δ-rays) produced by the electron track itself. More detailed break-downs can be found in [7]. The fraction is somewhat independent of electron $\mathrm{p_T}$ but decreases from $\approx$ 97% in 50 GeV $\mathrm{E_T}$ jets to $\approx$ 90% in 200 GeV $\mathrm{E_T}$ jets.

A study of hit merging probability is shown in Figure 14(b), where we report the fraction of hits in the reconstructed electron track that have not coalesced with neighbouring clusters and are required explicitly to be associated to electron impacts. The dependence of the hit sharing probability on jet $\mathrm{E_T}$ is noticeable. The fractions of track hits which are incorrectly associated or merged are comparable, as can be seen by comparing figures 14(a) and (b), and have a similar dependence on jet $\mathrm{E_T}$.

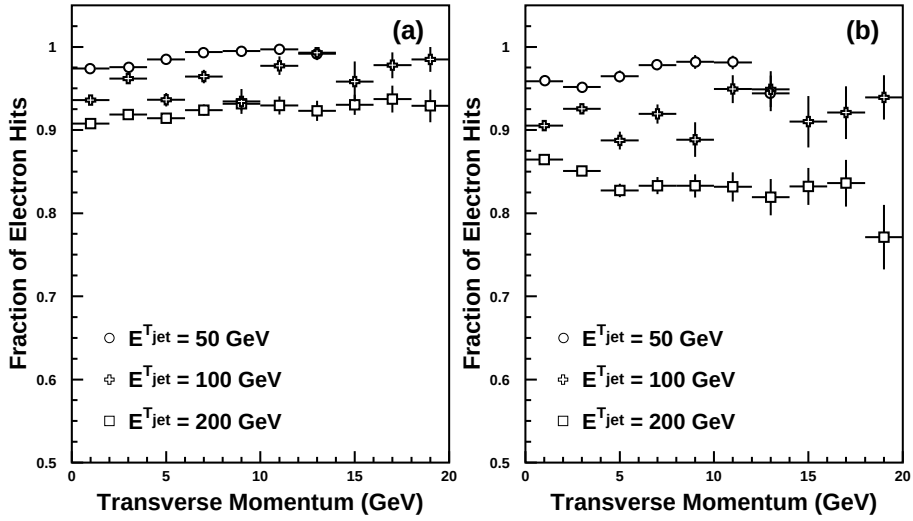

Figure 14: Fraction of hits of the reconstructed tracks associated to the generated electrons (as a function of track transverse momentum for different jet $\mathrm{E_T}$'s. The electron hits which have merged with other hits are (a) included, (b) not included in the list of electron hits. Fractions are defined with respect to the total number of hits on the track.

We have investigated the selection and rejection efficiencies during the high luminosity runs of LHC by overlaying a pile-up of 24 minimum bias interactions on top of the signal events ([4], Sec. 7.11). We have studied the large $\mathrm{E_T}$ b-jets sample ($\mathrm{E_T}$ = 200 GeV) for which the deterioration in electron selection efficiency is largest. Table 6 summarises selection efficiencies of 'electron' candidates for electron and non-electron tracks. The rejection efficiency is almost unchanged with respect to the low luminosity case (no pile-up), whereas the electron selection efficiency decreases from 90% to 80%. The reduction is due to spurious hit assignment to the track which is reconstructed by fitting a larger fraction of 'non-electron' hits. The fraction of electron hits used to fit the reconstructed track drops from 85% to 80%.

	e	μ	π	K	p
Preselected Tracks by ID	3018	309	19419	3323	1825
'Electron' Candidates	2440	0	519	53	39
Discrimination Efficiency (%)	80.8	100.0	97.3	98.4	97.9

Table 6: 'Electron' discrimination efficiency for different particle types in high luminosity $\mathrm{E_T}$ = 200 GeV $b\bar{b}$ jet events.

7 Summary

We have evaluated the performance of the CMS tracker in measuring the particle differential energy loss. From the measurements in the silicon detectors (pixel as well as the strip detectors), it is possible to obtain a discrimination of 1.5σ between π and K and larger than 5σ between e and μ.

The significance of the discrimination allowed us to evaluate the possible electron identification capability in CMS, using exclusively the tracking detector. We looked into two types of event samples: low momentum electron samples from B_s decays and high $\mathrm{E_T}$ $b\bar{b}$ jets for which the average track reconstruction efficiency ranges between 65-75%. Using rather simple criteria, in both cases one can get electron selection efficiencies in excess of 90% with 99% rejection capability. In very high luminosity LHC conditions, the electron selection efficiency drops to 80% with rejection capabilities in excess of 97%. This study estimates the asymptotic performance of the detector. Indeed a number of effects that can affect the $\mathrm{dE/dx}$ resolution have not been simulated and will be the object of farther study when beam test data will be available. Further, the energy calibration of the Tracking detector will present a hard challenge due to the very large number of readout channels. In this respect we would like to stress that a precise measurement of the sensor thickness would be a major contribution to the detector calibration. We propose then that the thicknesses should be measured during production phase and stored in the detector database. Notwithstanding these difficulties, the capability of identifying electrons of moderate and low $\mathrm{p_T}$, even within high $\mathrm{E_T}$ jets cores, can result to be an essential tool for data analysis. The large material budget of the tracker impairs the electron track reconstruction performance and the track finders can use significant $\mathrm{dE/dx}$ measurements which will help to define electron candidates. B-physics can profit of electron identification tools at low track $\mathrm{p_T}$, when the EM calorimeter is not fully performant. The capability to implement soft lepton b-jet tagging will be addressed in further studies.

References

[1] CMS Technical Proposal, CERN/LHCC 94-38, LHCC/P1, December 15, 1994.

[2] CMSIM User's Manual and Reference Guide, *http://cmsdoc.cern.ch/cmsim/cmsim.html*

[3] R. Brun $etal.$, *GEANT3 Users Guide.*, CERN Program Library W5013.

[4] CMS Tracker Technical Design Report, CERN/LHCC 98-6, CMS TDR 5, April 15, 1998.

[5] Particle Data Group, *http://pdg.lbl.gov/contents_other_hep.html*

[6] M. Maire, private communication.

[7] V. Ciulli $etal.$, *Study of a Very Large Pitch CMS Silicon Strip Detector.*, CMS IN 1999/025